Renewable Energy 178 (2021) 202–211

Contents lists available at ScienceDirect

Renewable Energy

journal homepage: www.elsevier.com/locate/renene

Non-fullerene organic photovoltaics based on thienopyrroledione comprising random copolymers; effect of alkyl chains

Mustafa Yasa [a, *], Tolga Depci [b], Eda Alemdar [c], Serife O. Hacioglu [d], Ali Cirpan [a, c, e, f], Levent Toppare [a, c, e, g]

[a] Department of Polymer Science and Technology, Middle East Technical University, 06800, Ankara, Turkey
[b] Department of Petrol and Natural Gases Engineering, Iskenderun Technical University, 31200, Hatay, Turkey
[c] Department of Chemistry, Middle East Technical University, 06800, Ankara, Turkey
[d] Department of Basic Sciences of Engineering, Faculty of Engineering and Natural Sciences, Iskenderun Technical University, 31200, Hatay, Turkey
[e] Center for Solar Energy Research and Applications, Middle East Technical University, 06800, Ankara, Turkey
[f] Department of Micro and Nanotechnology, Middle East Technical University, 06800, Ankara, Turkey
[g] Department of Biotechnology, Middle East Technical University, 06800 Ankara, Turkey

ARTICLE INFO

Article history:
Received 4 February 2021
Received in revised form
19 May 2021
Accepted 20 June 2021
Available online 21 June 2021

Keywords:
Random copolymers
Spacer
Thienopyrroledione
Benzodithiophene
Electrochemistry
Organic photovoltaics

ABSTRACT

Two new random donor-acceptor (D-A) copolymers, signed as P1 and P2, were designed and synthesized. Electrochemical and spectroelectrochemical measurements were performed to investigate absorption, energy levels, electronic and optical band gaps for comparison. The polymers were used as donor polymers in the active layer to fabricate non-fullerene, bulk heterojunction (BHJ) organic photovoltaics (OPVs). Investigations were carried out through the conventional BHJ structure; ITO/PEDOT: PSS/Active Layer/LiF/Al, where active layer consists of 3,9-bis(2-methylene-(3-(1,1-dicyanomethylene)-indanone))-5,5,11,11-tetrakis(4-hexylphenyl)-dithieno[2,3-d:2′,3′-d']-*s*-indaceno[1,2-b:5,6-b']dithiophene (ITIC) as the acceptor and thienopyrroledione containing donors. The device based on P1:ITIC(1:1) blend with a thickness of 161 nm gave the best performance with a power conversion efficiency (PCE) of 7.94%, an open-circuit voltage (V_{OC}) of 0.86 V, a short-current density (J_{SC}) of 18.45 mA cm^{-2} and a fill factor (FF) of 50.12%. The highest PCE obtained from P2 based organic solar cell is 1.96%. P2 exhibited low solubility attributed to the lack of alkyl groups enhancing polymer solubility, electronic properties, and photovoltaic performances. The research outputs exhibit that introduction of alkyl chains on the polymer backbone can enhance device performance.

1. Introduction

Conventional organic photovoltaics (OPVs) generally include a bulk heterojunction (BHJ) architecture, a blend of a donor, and an acceptor moiety. Absorption of light by this blend generates excitons splitting into free chargers [1–3]. Although OPVs bear various components, acceptor materials significantly define the solar cell device's power conversion efficiency (PCE) [4]. Fullerene derivatives with unsurpassed charge transport features and the superior ability to create phase separation in nanoscale in the blend led them to be utilized in the BHJ solar cells as promising acceptor moieties [5–8]. Although fullerene-based acceptors have these superior properties, there are various drawbacks, including the cost of purification and production, vulnerability to air, limited light absorption, and difficulties in adjusting optoelectronic properties. These aspects brought a challenge in increasing the PCE of OPVs [9–13]. Non-fullerene acceptors (NFAs) have caught great attention. Compared to fullerene derivatives, NFA molecules can be synthesized and purified easily via various functional groups that can adjust optoelectronic properties. In addition to the synthesis facilities, enhanced light absorption, morphology, and electronic properties eliminate fullerene derivatives acceptors [14,15]. Considering features as mentioned earlier (superior electronic and optical properties, ease of production, enhanced absorption), NFA-based organic photovoltaics have demonstrated higher power conversion efficiencies (PCE) than fullerene-based analogous during the past few years [16–18]. Compared to bilayer structure, BHJ provides an optimal domain size to enhance exciton dissociation by

* Corresponding author. Department of Polymer Science and Technology, Middle East Technical University, 06800, Ankara, Turkey.
E-mail address: mustafa.yasa@metu.edu.tr (M. Yasa).

https://doi.org/10.1016/j.renene.2021.06.087
0960-1481/

forming an ideal photoactive layer; a vicinal mixture of donor and acceptor [19].

Being rigid and symmetric, TPD can be easily modified to introduce various functional groups; subsequently, the solubility of polymers can be controlled. TPD has a strong electron-withdrawing feature attributed to the diimide nature. This results in lower band gap conjugated polymers via stabilizing the lowest unoccupied molecular orbital (LUMO). Besides, TPD, due to its quinoidal structure, can stabilize excited state energy. Therefore, TPD-containing conjugated polymers are supposed to exhibit high V_{OC} values [20–26]. It is well known that chalcogenophenes like selenophene, thiophene, and alkyl-substituted thiophene are introduced as π-spacer to tune frontier molecular orbital energy levels thus band gaps [27–33]. Conjugated polymers, including π-spacers, show red-shifted absorption [34].

An effective way of enhancing PCE values of polymer-based OPVs is alkyl side chain engineering. Such modifications improve not only the solubility properties of the polymers but also the morphology of the donor: acceptor blend through molecular aggregation; π–π stacking, which is crucial for the device performance [35,36]. Morphology of the active layer alters with the optimized selection of alkyl chain. While long alkyl chains provide large domain sizes, linear and branched alkyl chains control the positions of acceptor molecules in fullerene-based BHJ blends [37–39]. Very recently, Hou's group reported naphtho[2,3-c]thiophene-4,9-dione-based polymers substituted with branched alkyl chains. The polymers were used as donors in non-fullerene based BHJ OPVs. The study reveals the that alkyl chains cause a conjugated core distortion which results in formation of a better BHJ morphology, subsequently high PCEs [40].

Motivated by these aspects of non-fullerene acceptors and TPD moieties, our work focuses on the design and the fabrication of non-fullerene BHJ OPVs, and investigation of effect of alkyl chains on the device performance. Herein, we report two random copolymers used as the donors to fabricate NFA-based organic BHJ photovoltaics. Random copolymers were obtained via coupling the monomer with 2,5-dibromo-3-(2-Ethylhexyl)thiophene or 2,5-Dibromothiophene, and BDT(TiC8) through Stille Polycondensation. Recently, various reports revealed TPD-based conjugated polymers for the application of non-fullerene OPVs with PCEs exceeding from 7% to 16% [41–49]. Selenophene was introduced as a π-spacer between TPD and (BDT(TiC8) to tune optoelectronic properties. To further regulate these properties, thiophene, alkyl-substituted thiophene, and BDT(TiC8) were introduced as donors into the polymer backbone. Obtained random conjugated polymers were used as donor polymers in the active layer to fabricate non-fullerene, bulk heterojunction OPVs.

2. Experimental

2.1. Materials, methods, and instrumentation

BDT(TiC8) was purchased from SOLARMER. Compound **1 (thiophene-3,4-dicarboxylic acid)** and all other chemicals were purchased from Sigma-Aldrich and used without any further purifications. Structural analyses of the synthesized molecules were performed via NMR (Bruker Spectrospin Avance DPX-400) and attenuated total Reflectance-Fourier-transform infrared spectroscopy (ATR–FTIR) (Thermo Scientific Nicolet™ iS10 FTIR). Weight-average and number-average molecular weights (M_w, M_n) of the polymers were determined via size exclusion chromatography (SEC) (Shimadzu LC-20AD) in chloroform at 40 °C. Electrochemical and spectroelectrochemical measurements were performed with a three-electrode system. Indium tin oxide (ITO) was utilized as the working electrode. Platinum (Pt) wire was used as the counter electrode, and silver (Ag) wire was used as the reference electrode. Cyclic voltammograms of the polymer films were obtained implementing a GAMRY Reference 600 potentiostat while spectroelectrochemical measurements were performed with a PerkinElmer Lambda 25 UV–Vis spectrophotometer. To fabricate BHJ devices, ITO was used as the anode, PEDOT: PSS as the hole transport layer, lithium fluoride (LiF) as the cathode buffer layer, and aluminum (Al) was used as the cathode. Morphology investigations of polymer: acceptor blends were performed via Atomic Force Microscopy (AFM) (Veeco MultiMode V) and Transmission Electron Microscopy (TEM) (Tecnai G2 Spirit BioTWIN) techniques.

2.2. Synthesis of monomers and polymers

Preparation of **2 (1H,3H-thieno[3,4-c]furan-1,3-dione)**, **3 (5-(2-ethylhexyl)-4H-thieno[3,4-c]pyrrole-4,6(5H)-dione)**, **4 (1,3-dibromo-5-(2-ethylhexyl)-4H-thieno[3,4-c]pyrrole-4,6(5H)-dione)**, **5 (1,3-dibromo-5-(2-ethylhexyl)-4H-thieno[3,4-c]pyrrole-4,6(5H)-dione)** and **6 (tributyl(selenophen-2-yl)stannane)** were previously reported [50]. Compound **7** and **TSeBr** were prepared according to the literature [51,52]. Scheme 1 represents the synthetic route for **TSeBr**, **P1** and **P2**.

2.2.1. 5-(2-ethylhexyl)-1,3-di(selenophen-2-yl)-4H-thieno[3,4-c] pyrrole-4,6(5H)-dione (7)

Under argon, **5** (0.3 g, 0.7 mmol) and tetrakis(-triphenylphosphine)palladium(0) (0.09 g, 0.08 mmol) were dissolved in dry toluene (25 mL). After the mixture reached 50 °C **6** (0.9 g, 2.14 mmol) was added in one portion. Following 17 h stirring at 110 °C, the reaction mixture was cooled to ambient temperature, and the solvent was removed under reduced pressure. Compound **7** was obtained by purification via chromatography (SiO_2, hexane: dichloromethane, 1:1). Yield: 0.27 g, 75%.

^{1}H NMR (400 MHz, $CDCl_3$): δ: 8.21 (d, J = 5.6 Hz, 2H), 7.93 (d, J = 3.9 Hz, 2H), 7.33 (m, 2H), 3.55 (d, J = 7.4 Hz, 2H), 1.88–1.82 (m, 1H), 1.42–1.25 (m, 8H), 0.87–0.93 (m, 6H).

^{13}C NMR (100 MHz, $CDCl_3$): δ: 163, 138.82, 136.39, 135.64, 131.57, 130.19, 127.53, 41.92, 38.04, 31.34, 28.39, 23.72, 22.59, 14.50, 10.35.

2.2.2. TSeBr

Compound 7 (0.25 g, 0.48 mmol) was dissolved in $CHCl_3$, (15 mL) under nitrogen. *N*-bromosuccinimide (0.22 g, 1.2 mmol) was added in one portion. The reaction mixture was stirred overnight at ambient temperature and monitored by thin-layer chromatography. After completing the reaction, the mixture was washed with water, and organic fractions were dried over Mg_2SO_4. Chloroform was removed under reduced pressure, and the target product was isolated by column chromatography on silica gel (SiO_2, hexane: dichloromethane, 4:1). Yield: 0. 25 g, 77%.

^{1}H NMR (400 MHz, $CDCl_3$): δ: 7.43 (d, J = 4.43 Hz, 2H), 7.21 (d, J = 4.43 Hz, 2H), 3.47 (d, J = 7.4 Hz, 2H), 1.82–1.76 (m, 1H), 1.38–1.22 (m, 8H), 0.9 (q, 6H).

^{13}C NMR (100 MHz, $CDCl_3$): δ: 162.8, 138.0, 137.6, 133.3, 130.7, 127.8, 122.5, 42.4, 38.1, 30.4, 28.4, 23.8, 23.0, 14.0, 10.3.

2.3. Polymer syntheses

TSeBr (73.4 μmol, 1 eq.), BDT(TiC8) (147 μmol, 2 eq.), P(o-tol)$_3$ (50 μmol, 0.68 eq.) and $Pd_2(dba)_3$ (16 μmol, 0.22 eq.) were introduced to a 25 mL Schlenk tube which was charged with a magnet bar, set up in an oil bath and connected to a vacuum-gas manifold. Following 1 h of vacuuming, Schlenk was provided with argon for the rest. Dry toluene (10 mL) was added to the mixture. The reaction mixture was heated up to 50 °C and followed by the addition of 2,5-dibromo-3-(2-ethylhexyl)thiophene or 2,5-dibromothiophene

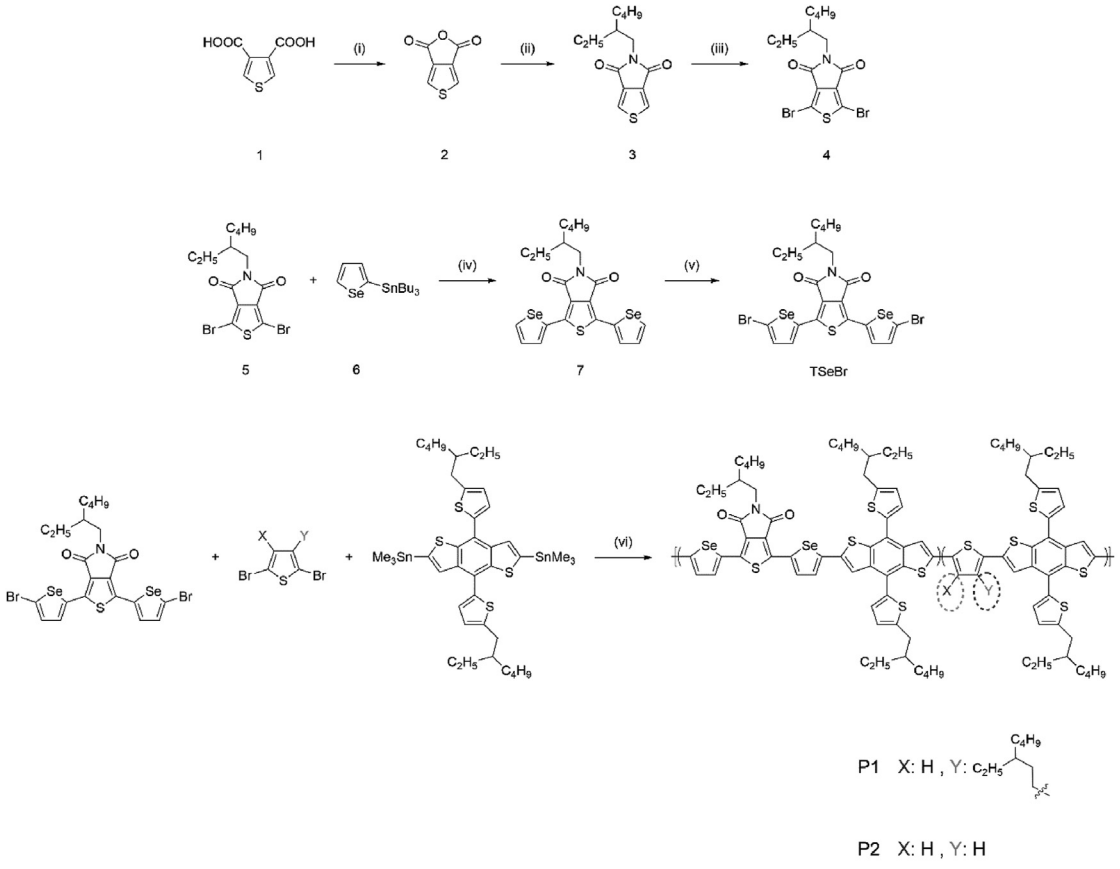

Reaction conditions; (i) Ac_2O, 140 °C, 24 h; (ii) 2-Ethylhexylamine, toluene, 115 °C, 24 h, $SOCl_2$, 75 °C, 3 h; (iii) TFA, H_2SO_4, NBS, room temperature, 24 h; (iv) $Pd(PPh_3)_4$, toluene, 115 °C, 17 h; (v) NBS, chloroform, overnight; (vi) $Pd_2(dba)_3$, P(o-tol)$_3$, toluene, 115 °C, 40 h

Scheme 1. Synthetic pathways for TSeBr, P1, and P2.

(73.4 μmol, 1 eq.). The reaction temperature was set to 100 °C. The completion of the reaction was monitored by thin-layer chromatography. After stirring 24h, the reaction mixture was allowed to cool down. The solvent was removed under reduced pressure. Cold methanol (100 mL) was added to the crude product. For the removal of catalytic residue, sodium diethyldithiocarbamate trihydrate (15 mg) was added. The mixture was stirred for 1 h and subjected to Soxhlet extractor, and washed with acetone, hexane, chloroform, and chlorobenzene. Low molecular weight fractions were removed with acetone and hexane. Both **P1** and **P2** were isolated in chloroform. Solvents were removed under reduced pressure, and **P1** (Yield: 125 mg, 91%) and **P2** (Yield: 80 mg, 62%) were obtained as dark purple crystals following recrystallization from methanol. M_n, M_w and PDI values for the two polymers are shown in Table 1.

2.4. OPV fabrication

For the fabrication of OPVs, a conventional BHJ device structure was built; ITO/PEDOT: PSS/Active Layer/LiF/Al. ITO-coated glass substrates were cleaned several times; ultra-sonication with toluene, detergent, water, and isopropyl alcohol (IPA), respectively. Following ultra-sonication, ITO-coated glass substrates were exposed to oxygen plasma for 5 min to remove organic contaminations and tune work function [53]. Polymer: acceptor blends were coated by spin coating in N_2 filled glove box. LiF (0.6 nm) and Al (100 nm) were evaporated at low pressure (~10^{-6} mbar) under vacuum. Current density vs. voltage measurements were performed by a Keithley 2400 digital source meter under AM 1.5 G solar radiation simulated at 100 mW cm^{-2}. External quantum efficiency (EQE) measurements were carried out with monochromatic light.

Table 1
Molecular weights and PDI values of the polymers.

Polymer	Number-average (M_n), kDa	Weight-average (M_w), kDa	PDI
P1	11	35	3.18
P2	4.8	9.2	1.91

3. Results

3.1. Electrochemical and spectroelectrochemical studies

Highest Occupied Molecular Orbital (HOMO) and Lowest Unoccupied Molecular Orbital (LUMO) energy levels and band gap values are of great importance for conjugated polymers since they affect their applicability in different application fields like organic photovoltaics and electrochromic devices. In order to investigate the redox behaviors and HOMO/LUMO energy levels of the resulting polymers, cyclic voltammetry (CV) studies were performed, and corresponding voltammograms were depicted in Fig. 1. Due to its certain simplicity and easy use, the CV technique was preferred for electrochemical analysis. Both P1 and P2 were dissolved in $CHCl_3$

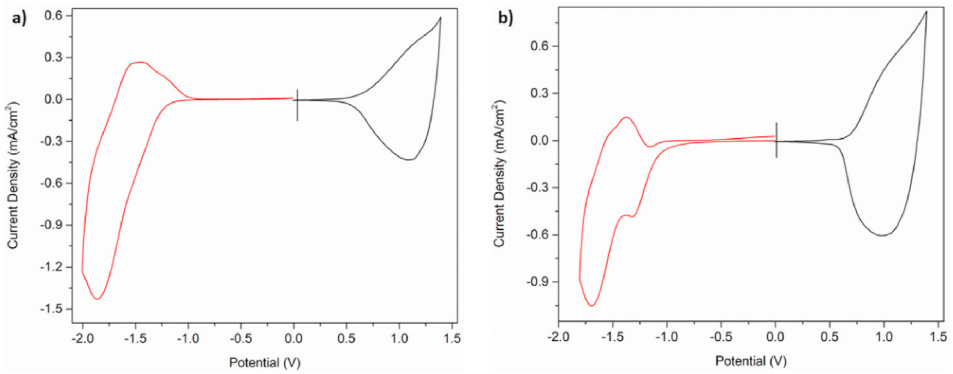

Fig. 1. Single scan cyclic voltammograms of (a) P1 and (b) P2 on ITO electrode in 0.1 M $TBAPF_6$/ACN electrolyte/solvent couple at a scan rate of 100 mV/s.

(5 mg. mL^{-1}) and spray-coated on an ITO glass electrode. Single scan cyclic voltammetry of the polymer films was performed in the potential range between −2.0 V and 1.4 V for P1 and between −1.8 V and 1.4 V for P2 in 0.1 M tetrabutylammonium hexafluorophosphate; $TBAPF_6$/ACN, electrolyte/solvent couple.

As illustrated in Fig. 1, both P1 and P2 exhibited ambipolar character, i.e., polymers have both p-type and n-type doping behaviors. While P1 has reversible oxidation/reduction peaks at 1.15 V and at −1.52/-1.85 V, P2 exhibits reversible oxidation/reduction peaks at 1.04 V and −1.31/-1.69 V in the anodic region and the cathodic region. HOMO/LUMO energy levels of both P1 and P2 were calculated by using the oxidation and reduction onset values determined from CVs. Due to the ambipolar characteristics of the two polymers, HOMO/LUMO energy levels were calculated from the oxidation/reduction onset potentials as −5.38 eV/-3.52 eV for P1 and as −5.43 eV/−3.69 eV for P2, respectively.

In order to examine the relation between the current density and the scan rate, single scan cyclic voltammograms were recorded at five different scan rates (50 mV/s, 100 mV/s, 150 mV/s, 200 mV/s, 250 mV/s) and corresponding current density versus scan rate graphs were illustrated in Fig. 2a. As seen in Fig. 2b, a linear dependence of current density to the scan rate shows the non-diffusion controlled reversible oxidation/reduction processes.

3.2. Spectroelectrochemistry

Spectroelectrochemical analyses were carried out to examine the changes in the optical properties of P1 and P2 via stepwise oxidation. A potentiostat integrated UV−Vis spectrophotometer was used during spectroelectrochemical studies, and progressively increasing potentials were applied while recording UV−Vis spectra. Similar to the electrochemical studies initially, polymers were dissolved in $CHCl_3$ and spray-coated on ITO-coated glass electrodes. They were dipped into 0.1 M $TBAPF_6$/ACN solutions to perform the spectroelectrochemical analysis. Neutral state absorptions were recorded at constant potentials (0.0 V) before the stepwise oxidation. Then electronic absorption spectra were recorded upon stepwise oxidation for both polymers (Fig. 3). During stepwise oxidation, while the neutral state absorption bands were decreasing, new absorption bands appeared at 830 nm and 835 nm, which can be dedicated to the formation of radical cations.

As illustrated in Fig. 3, neutral state absorptions were recorded at 571 nm and 576 nm for P1 and P2, corresponding to the π-π* transitions. The optical band gap values (E^{opt}_g) of P1 and P2 were calculated from the onset of the neutral state absorption according to the equation $E^{opt}_g = 1241/\lambda$. As summarized in Table 2, the E^{opt}_g values were calculated as 1.78 eV and 1.69 eV for P1 and P2, respectively. All electrochemical and spectroelectrochemical analyses were summarized in Table 2.

Following electrochemical and spectroelectrochemical characterizations, the optical properties of the polymers were also investigated both in the thin film form and in $CHCl_3$ solution. As seen in Fig. 4, polymers have strong absorptions in the visible region between 400 nm and 700 nm. The maximum absorptions are located at 561/571 nm, and 534/576 nm in solution and in thin film forms for P1 and P2, respectively. As seen, 10 nm and 42 nm red-shifts were observed in the absorption spectra, which can be dedicated to the higher conjugation length and intermolecular interaction between polymer chains in the solid state.

Furthermore, another important application field for conjugated polymers is electrochromic device applications. For these applications colors and parameters like switching time and optical contrast of the resulting polymers are essential. In Fig. 5, the colors of both P1 and P2 recorded in the neutral, oxidized, and reduced states are illustrated. Both polymers showed multichromic behavior and exhibited varying tones of purple in the neutral states (neutral state absorptions recorded at 571 nm and 576 nm) with gray-colored oxidized states and grayish-blue colored reduced states.

3.3. Kinetic studies

As mentioned before, kinetic studies were performed in order to record and analyze the optical contrast and switching time values which are crucial especially for the electrochromic performances of resulting polymers. For that purpose, a square-wave potential method was used by applying potentials between two extreme states (oxidized/reduced states) with 5 s time intervals at λ_{max} values located at 570 nm/830 nm for P1 and 575 nm/835 nm for P2.

As a result of electrochromic switching studies, percent transmittance against time graphs were recorded and illustrated in Fig. 6 for P1 and P2, respectively. Percent transmittance changes were determined as 23% at 570 nm, 29% at 830 nm for P1, and 20% at 575 nm, 40% at 835 nm for P2. The time required for one complete switch between two extreme states could be defined as switching time, and for P1 and P2, these values were calculated as 1.8 s, 2.0 s, and 2.9 s, 3.7 s at their corresponding wavelengths, respectively. All electrochromic switching results were summarized in Table 3.

3.4. OPV studies

The fabrication procedure for OPV devices were explained in detail in section 2.4. The active layer consists of the non-fullerene acceptor, ITIC, and thienopyrroledione containing donors, **P1** or **P2**. Various optimization studies (solvent selection, determination of donor: acceptor ratio, active layer's mass ratio optimizations,

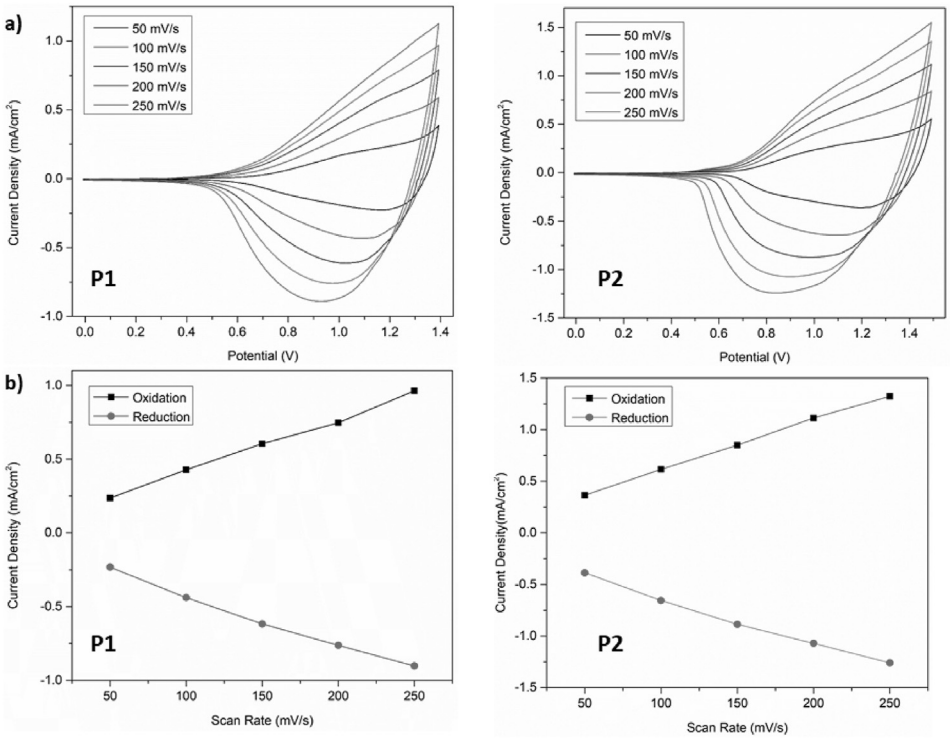

Fig. 2. Single scan cyclic voltammograms of (a) P1 and P2, (b) current density versus scan rates curves of P1 and P2 at five different scan rates (50 mV/s, 100 mV/s, 150 mV/s, 200 mV/s, 250 mV/s).

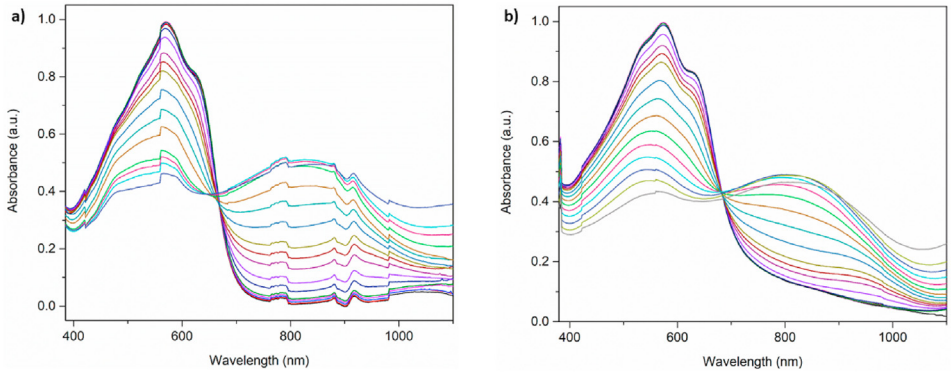

Fig. 3. Electronic absorption spectra of P1 and P2 in 0.1 M $TBAPF_6$/ACN solution between 0.0 V and 1.4 V for P1 (a), 0.0 V and 1.4 V for (b) P2.

Table 2
Electrochemical properties of P1 and P2

	$E_{p\text{-doping}}$ (V)	$E^{onset}{}_{p\text{-doping}}$ (V)	$E_{n\text{-doping}}$ (V)	$E^{onset}{}_{n\text{-doping}}$ (V)	HOMO (eV)	LUMO (eV)	E_g^{op} (eV)	λ_{max} (nm)	Polaron (nm)
P1	1.15	0.63	−1.52/-1.85	−1.23	−5.38	−3.52	1.78	571/630	830
P2	1.04	0.68	−1.31/-1.69	−1.06	−5.43	−3.69	1.69	576/631	835

determination of the active layer's thickness, additive selection (diphenyl ether; DPE, 1-chloronaphthalene; CN and 1, 8-diiodooctane; DIO) and thermal annealing) were carried out to obtain the best performance from the devices. As a result of the optimizations, the mass ratio was determined as 30 mg. mL^{-1}. Polymer (P1 or P2): Acceptor (ITIC) blend was dissolved in chlorobenzene (CB). Active layers were spin-coated with a rate of 2000 rpm for 30 s from ITIC: Polymer blends with and without solvent additive in N_2 filled glove box. LiF (0.6 nm) and Al (100 nm) were evaporated at low pressure (~10^{-6} mbar) in a vacuum environment. Fig. 7 represents the energy diagram and the bulk heterojunction OPVs' device architecture.

J-V curves of the best devices are shown in Fig. 8, and the photovoltaic parameters are summarized in Table 4. The best performance of the **P1**: ITIC blend with the thickness of 161 nm was obtained by coating the active layer with 1: 1 Polymer: ITIC ratio, and 7.94% PCE was obtained. Although the addition of additives is intended to improve film morphology, no improvement has been

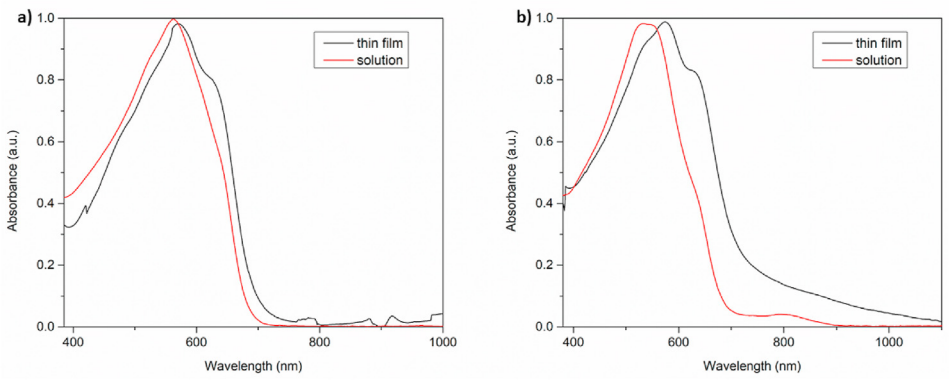

Fig. 4. Electronic absorption spectra of (a) P1, (b) P2 in thin film form and in chloroform.

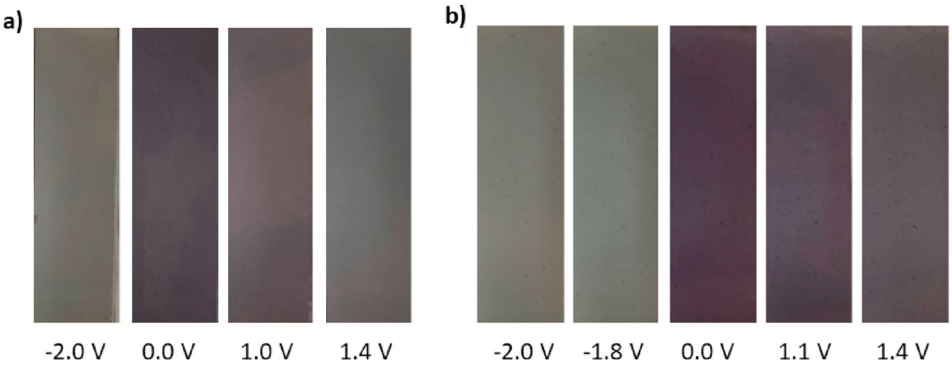

Fig. 5. Colors of (a) P1, (b) P2 at neutral and oxidized/reduced states with intermediate colors

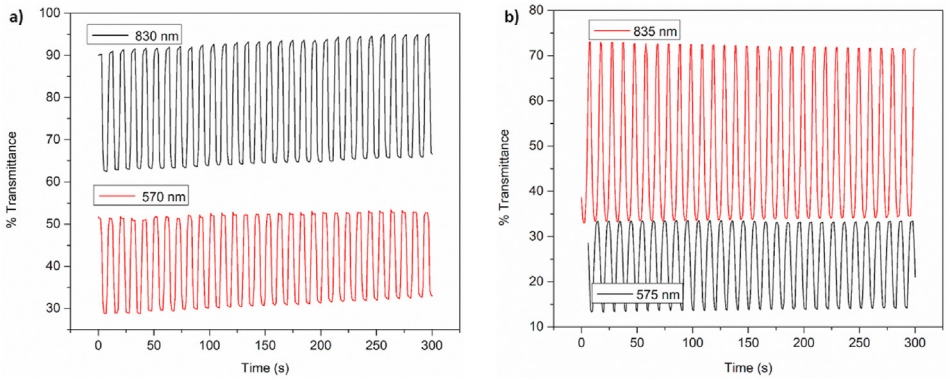

Fig. 6. Percent transmittance changes for (a) P1 at 570 nm and 830 nm and for (b) P2 at 575 nm and 835 nm in 0.1 M $TBAPF_6$/ACN solution.

Table 3
Kinetic properties of P1 and P2

		Optical Contrast (%)	Switching Time (s)
P1	570 nm	23	1.8
	830 nm	29	2.0
P2	575 nm	20	2.9
	835 nm	40	3.7

observed. As for **P2** based OPVs, CB was also seen as the best working solvent. The highest PCE achieved in the **P2** based OPV with a thickness of 106 nm was obtained by coating the active layer with a mass ratio of 1:1.5 at 2000 rpm, which is 1.96%. **P2** exhibited solubility problems due to a lack of alkyl chains, proving that the alkyl chain's introduction to the polymer's backbone enhances polymer solubility and electronic properties, hence photovoltaic performances [54]. P1 based OPVs exhibit superior performances than P2 based ones because the M_n value of P2 was deficient compared to P1. As well known in the literature, our study also proves that the M_n affects the microstructure morphology and consequently PCE [55]. This effect is explained in the TEM images in the active layer section. Theoretical V_{OC} of all-polymer solar cells is deduced from the difference between E_{LUMO} of the acceptor and E_{HOMO} of the donor. While the V_{OC} value of P1 OPVs is precisely the same as expected (can be calculated from Eq. (1)), the V_{OC} value of P2 based OPVs is lower than the theoretical value due to energetic

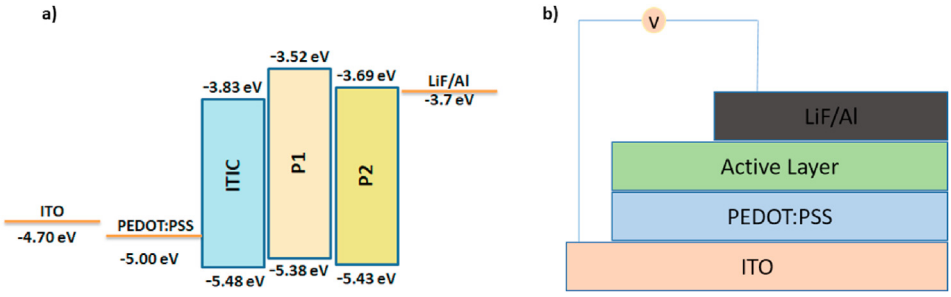

Fig. 7. (a) Schematic energy level diagram and (b) device architecture of OPVs.

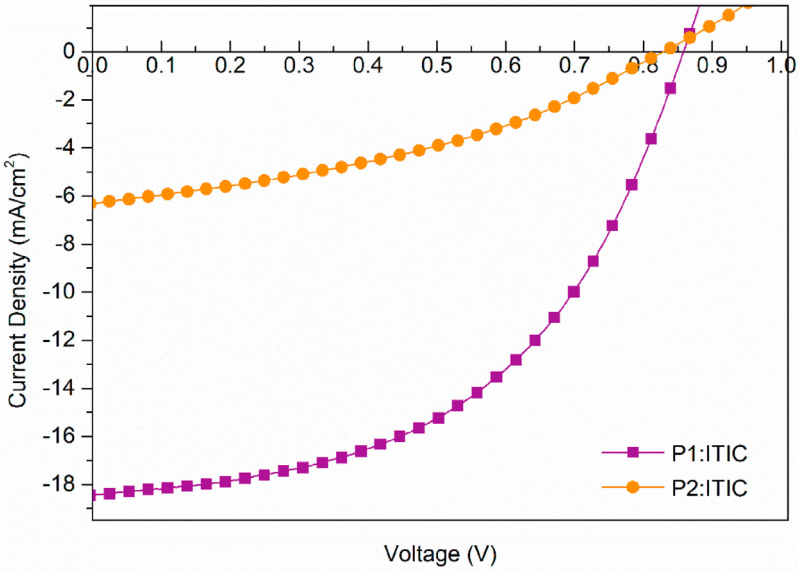

Fig. 8. Current-voltage characteristics of P1: ITIC and P2: ITIC devices under AM 1.5 G solar simulator.

Table 4
Photovoltaic parameters of P1:ITIC and P2:ITIC devices.

Polymer	Solvent	Weight (%)	Polymer: ITIC	V_{oc} (V)	J_{sc} (mA.cm^{-2})	PCE (%)	FF (%)	Treatment
P1	CB	3	1:1.5	0.87	15.26	7.09	53.4	–
P1	**CB**	**3**	**1:1**	**0.86**	**18.45**	**7.94**	**50.12**	**-**
P1	CB	3	1:0.8	0.85	16.87	5.94	41.38	–
P1	ODCB	3	1:1.5	0.88	8.54	4.56	60.9	–
P1	CB	3	1:1	0.88	15.69	5.99	43.21	1% CN
P2	**CB**	**3**	**1:1.5**	**0.83**	**6.31**	**1.96**	**37.44**	**-**
P2	ODCB	3	1:1.5	0.74	3.75	1.26	45.41	–

disorder at the charge transport level [56]. P1 based OPVs displays better performances than P2 based OPVs, mainly profiting the higher Voc of 0.86 V and FF of 50.12%. All these findings can be supported by the fact that P1 has higher crystallinity than P2; The higher the crystallinity, the greater the tendency to self-aggregate, and the larger the field size in thin films with very high charge mobility [57].

$$V_{OC} = (1/e)\left(\left|E^{HOMO}_{Donor} - E^{LUMO}_{Acceptor}\right|\right) - 0.3\ V \qquad \text{Eq. 1}$$

AFM images were recorded to examine the films' topographies. Fig. 9 shows AFM images, both 2D and 3D images, proving how uniformly coated the films are. P2 based OPVs, a rough surface image, and the non-uniform coating are seen in the 3D image of P2 based OPV, which already has a dissolution problem. The surface roughness of the P2:ITIC blend was the largest among others (Fig. 9b).

The TEM images were examined to obtain more in-depth information about morphology (Fig. 10). The ideal morphology formed in the active layer provides suitable interfaces for efficient charge separation and promising percolation pathways for charge carrier transport to the respective electrodes to minimize free charge recombination [58]. For the blend P1:ITIC (Fig. 10a), ITIC is dispersed so uniformly throughout the film, and percolations are thinner and precise. However, for the P2:ITIC blend (Fig. 10b), phase separation is so apparent that large aggregates of ITIC (dark areas) are trapped within the polymer matrix. These aggregates are thought to interrupt charge transport and thus resulting in reducing device performance [59]. Addition of 1% of CN to P1:ITIC solution, FF value decreases considerably (Table 4). TEM images

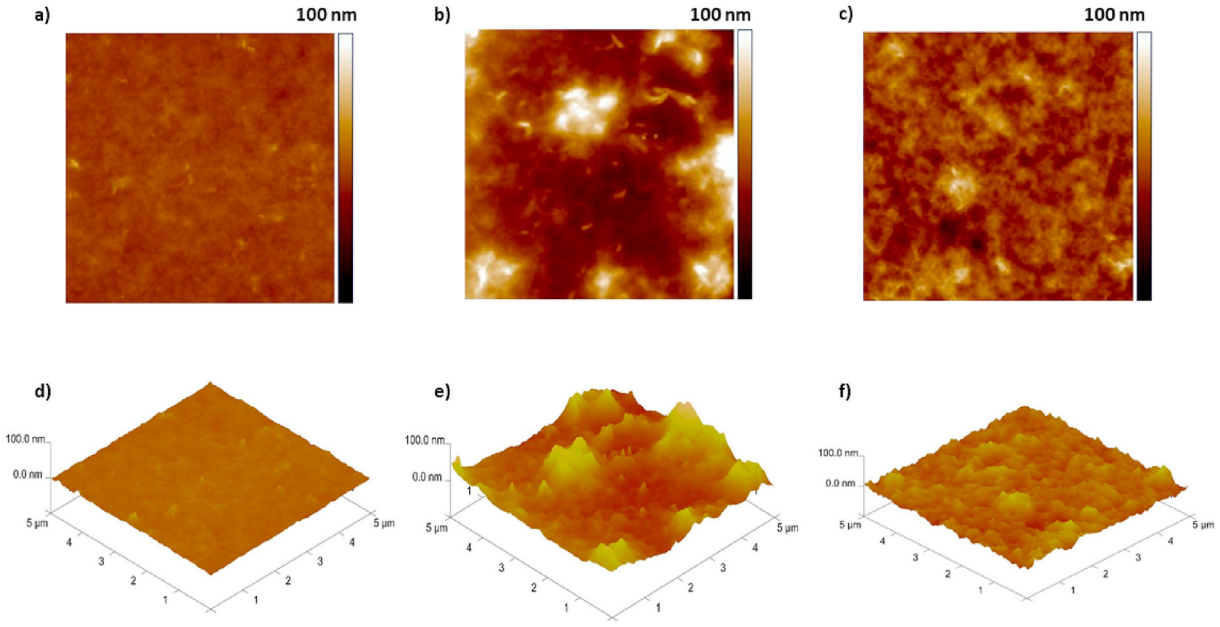

Fig. 9. 2D AFM images of (a) P1:ITIC, (b) P2:ITIC, (c) P1:ITIC w/1% CN and 3D AFM images of (d) P1:ITIC, (e) P2:ITIC, (f) P1:ITIC w/1% CN.

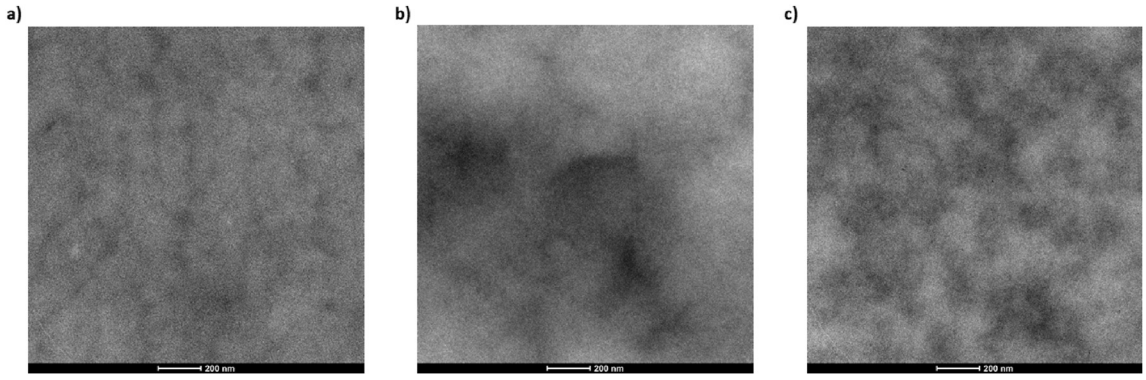

Fig. 10. TEM images of (a) P1:ITIC, (b) P2:ITIC, (c) P1:ITIC w/1% CN.

were used to understand the reason for this severe decrease. Comparing Fig. 10a and c, the latter shows large-scale phase separation, resulting in less charge carrier photogeneration and hindered transport, finally decreasing photovoltaic properties [60].

The incident photon to electron conversion efficiency (IPCE) was studied to confirm the best device's photoresponse, as shown in Fig. 11. The photocurrent response for both polymers was performed between 300 nm and 900 nm. The highest IPCE value for P1 and P2 reached 82% and 26%, respectively. The results obtained from the EQE curve are consistent with J_{SC} values in Table 4.

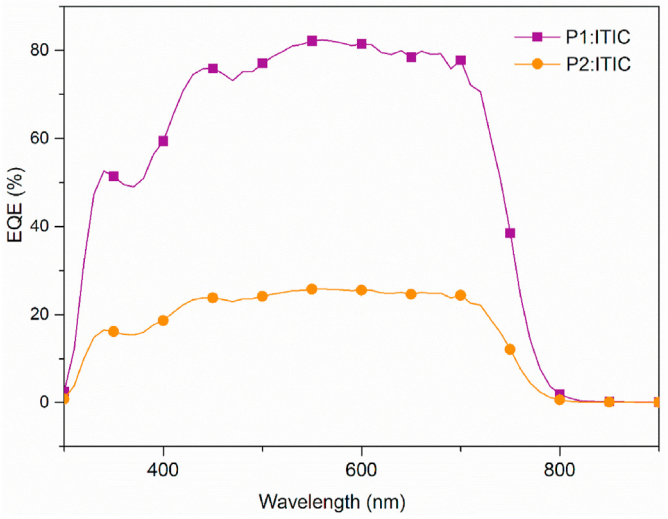

Fig. 11. EQE curves of P1: ITIC and P2: ITIC devices.

4. Conclusions

In this study, two new random copolymers containing TPD as the core unit were synthesized. P1 containing alkyl thiophene has a larger molecular weight than P2 which is attributed to the lack of alkyl chain, which enhances the solubility of the polymer. The electrochemical and spectroelectrochemical properties of the two polymers were investigated. TPD as an acceptor moiety enhanced V_{OC} values and provided deep HOMO levels, subsequently better OPV performances. The best result was obtained with the device based on P1: ITIC with a PCE of 7.94%, a J_{SC} value of 18. 45 mA cm^{-2}

and with an FF value of 50.12%. P2 based devices exhibited comparatively lower PCEs (1.96% max) and other OPV parameters. We believe that the lower molecular weight of P2 disturbed film morphology of the polymer: acceptor blend, which is supported by AFM and TEM images. Thus, P1 exhibited relatively better OPV performances. Our study represents a synthetic approach to exhibit the effect of alkyl chains on device performance based on TPD containing random copolymers and NFAs. Previously reported studies support that new TPD-containing random copolymers and NFA-based organic photovoltaics exhibit better PCEs compared to their fullerene-based counterparts [61–66].

Declaration of competing interest

The authors declare that they have no known competing financial interests or personal relationships that could have appeared to influence the work reported in this paper.

References

[1] S.E. Shaheen, C.J. Brabec, N.S. Sariciftci, F. Padinger, T. Fromherz, J.C. Hummelen, 2.5% efficient organic plastic solar cells, Appl. Phys. Lett. 78 (2001) 841–843, https://doi.org/10.1063/1.1345834.

[2] S. Gu, H. Neugebauer, N.S. Sariciftci, Conjugated polymer-based organic solar cells, Chem. Rev. (2007) 1324–1338, https://doi.org/10.1021/cr050149z.

[3] K. Ramki, N. Venkatesh, G. Sathiyan, R. Thangamuthu, P. Sakthivel, A comprehensive review on the reasons behind low power conversion efficiency of dibenzo derivatives based donors in bulk heterojunction organic solar cells, Org. Electron. 73 (2019) 182–204, https://doi.org/10.1016/j.orgel.2019.05.047.

[4] A. Armin, W. Li, O.J. Sandberg, Z. Xiao, L. Ding, J. Nelson, D. Neher, K. Vandewal, S. Shoaee, T. Wang, H. Ade, T. Heumüller, C. Brabec, P. Meredith, A history and perspective of non-fullerene electron acceptors for organic solar cells, Adv. Energy Mater. 20003570 (2021) 1–42, https://doi.org/10.1002/aenm.202003570.

[5] D. Rodriquez, S. Savagatrup, E. Valle, C.M. Proctor, C. Mcdowell, G.C. Bazan, T. Nguyen, D.J. Lipomi, Mechanical properties of solution-processed small-molecule semiconductor films, ACS Appl. Mater. Interfaces (2016), https://doi.org/10.1021/acsami.6b02603.

[6] Y. He, H.Y. Chen, J. Hou, Y. Li, Indene - C60 bisadduct: a new acceptor for high-performance polymer solar cells, J. Am. Chem. Soc. 132 (2010) 1377–1382, https://doi.org/10.1021/ja908602j.

[7] A. Celik Bedeloglu, A. Demir, Y. Bozkurt, N.S. Sariciftci, Photovoltaic properties of polymer based organic solar cells adapted for non-transparent substrates, Renew. Energy 35 (2010) 2301–2306, https://doi.org/10.1016/j.renene.2010.02.030.

[8] D. Roy, B. Shastri, M. Imamuddin, K. Mukhopadhyay, K.U.B. Rao, Nano-structured carbon and polymer materials - synthesis and their application in energy conversion devices, Renew. Energy 36 (2011) 1014–1018, https://doi.org/10.1016/j.renene.2010.09.010.

[9] I. Riedel, N. Martin, F. Giacalone, J.L. Segura, D. Chirvase, J. Parisi, V. Dyakonov, Polymer solar cells with novel fullerene-based acceptor, Thin Solid Films (2004) 451–452, https://doi.org/10.1016/j.tsf.2003.10.088, 43–47.

[10] I. Donor, acceptor, internal donor-acceptor, science 270 (80-) (1995) 1–3. http://science.sciencemag.org/.

[11] M. Solá, J. Mestres, J. Martí, M. Duran, An AM1 study of the reactivity of buckminsterfullerene (C60) in a Diels-Alder model reaction, Chem. Phys. Lett. 231 (1994) 325–330, https://doi.org/10.1016/0009-2614(94)01249-0.

[12] H. Seyler, W.W.H. Wong, D.J. Jones, A.B. Holmes, Continuous flow synthesis of fullerene derivatives, J. Org. Chem. 76 (2011) 3551–3556, https://doi.org/10.1021/jo2001879.

[13] Z. Hu, J. Zhang, L. Huang, J. Sun, T. Zhang, H. He, J. Zhang, H. Zhang, Y. Zhu, Natural drying effect on active layer for achieving high performance in polymer solar cells, Renew. Energy 74 (2015) 11–17, https://doi.org/10.1016/j.renene.2014.07.034.

[14] L. Duan, N.K. Elumalai, Y. Zhang, A. Uddin, Progress in non-fullerene acceptor based organic solar cells, Sol. Energy Mater. Sol. Cells 193 (2019) 22–65, https://doi.org/10.1016/j.solmat.2018.12.033.

[15] Y. Zang, C.Z. Li, C.C. Chueh, S.T. Williams, W. Jiang, Z.H. Wang, J.S. Yu, A.K.Y. Jen, Integrated molecular, interfacial, and device engineering towards high-performance non-fullerene based organic solar cells, Adv. Mater. 26 (2014) 5708–5714, https://doi.org/10.1002/adma.201401992.

[16] H. Zhang, H. Yao, J. Hou, J. Zhu, J. Zhang, W. Li, R. Yu, B. Gao, S. Zhang, J. Hou, Over 14% efficiency in organic solar cells enabled by chlorinated nonfullerene small-molecule acceptors, Adv. Mater. 30 (2018) 1–7, https://doi.org/10.1002/adma.201800613.

[17] L. Meng, Y. Zhang, X. Wan, C. Li, X. Zhang, Y. Wang, X. Ke, Z. Xiao, L. Ding, R. Xia, H.L. Yip, Y. Cao, Y. Chen, Organic and solution-processed tandem solar cells with 17.3% efficiency, Science 361 (80-) (2018) 1094–1098, https://doi.org/10.1126/science.aat2612.

[18] J. Sun, X. Ma, Z. Zhang, J. Yu, J. Zhou, X. Yin, L. Yang, R. Geng, R. Zhu, F. Zhang, W. Tang, Dithieno[3,2-b:2′,3′-d]pyrrol fused nonfullerene acceptors enabling over 13% efficiency for organic solar cells, Adv. Mater. 30 (2018) 1–8, https://doi.org/10.1002/adma.201707150.

[19] J. Chen, Y. Chen, L.-W. Feng, C. Gu, G. Li, N. Su, G. Wang, S.M. Swick, W. Huang, X. Guo, A. Facchetti, T.J. Marks, Hole (donor) and electron (acceptor) transporting organic semiconductors for bulk-heterojunction solar cells, Energy 2 (2020) 100042, https://doi.org/10.1016/j.enchem.2020.100042.

[20] S.M. Bang, J. hyun Park, S. Kang, Y.S. Lee, B. Lim, H. Heo, J. Lee, Y. Lee, S.I. Na, Thienopyrroledione and benzodithiophene/thiophene-based random terpolymer for polymer solar cells with improved fill factor, Dyes Pigments 140 (2017) 229–235, https://doi.org/10.1016/j.dyepig.2017.01.049.

[21] K.W. Song, M. hee Choi, M. hee Han, D.K. Moon, Open circuit voltage increase by substituted spacer and thieno[3,4-c]pyrrole-4,6-dione for polymer solar cells, J. Ind. Eng. Chem. 20 (2014) 426–434, https://doi.org/10.1016/j.jiec.2013.04.037.

[22] C. Piliego, T.W. Holcombe, J.D. Douglas, C.H. Woo, P.M. Beaujuge, J.M.J. Fréchet, Synthetic control of structural order in N-alkylthieno[3,4- c]pyrrole-4,6-dione-based polymers for efficient solar cells, J. Am. Chem. Soc. 132 (2010) 7595–7597, https://doi.org/10.1021/ja103275u.

[23] M.C. Yuan, M.Y. Chiu, S.P. Liu, C.M. Chen, K.H. Wei, A thieno[3,4-c]pyrrole-4,6-dione-based donor-acceptor polymer exhibiting high crystallinity for photovoltaic applications, Macromolecules 43 (2010) 6936–6938, https://doi.org/10.1021/ma101523a.

[24] Q. Zheng, B.J. Jung, J. Sun, H.E. Katz, Ladder-type oligo- p -phenylene-containing copolymers with high open-circuit voltages and ambient photovoltaic activity, J. Am. Chem. Soc. 132 (2010) 5394–5404, https://doi.org/10.1021/ja909111p.

[25] Y. Zhang, S.K. Hau, H.L. Yip, Y. Sun, O. Acton, A.K.Y. Jen, Efficient polymer solar cells based on the copolymers of benzodithiophene and thienopyrroledione, Chem. Mater. 22 (2010) 2696–2698, https://doi.org/10.1021/cm100417z.

[26] Y. Zou, A. Najari, P. Berrouard, S. Beaupré, B. Réda Aïch, Y. Tao, M. Leclerc, A thieno[3,4- c]pyrrole-4,6-dione-based copolymer for efficient solar cells, J. Am. Chem. Soc. 132 (2010) 5330–5331, https://doi.org/10.1021/ja101888b.

[27] D. Liu, B. Kan, X. Ke, N. Zheng, Z. Xie, D. Lu, Y. Liu, Extended conjugation length of nonfullerene acceptors with improved planarity via noncovalent interactions for high-performance organic solar cells, Adv. Energy Mater. 8 (2018) 1–8, https://doi.org/10.1002/aenm.201801618.

[28] S. Agbolaghi, Well-functioned photovoltaics based on nanofibers composed of PBDT-TIPS-DTNT-DT and graphenic precursors thermally modified by polythiophene, polyaniline and polypyrrole, Polym. Int. 68 (2019) 1516–1523, https://doi.org/10.1002/pi.5859.

[29] R.K. Gunasekaran, P.J.S. Rana, S.H. Park, V. Tamilavan, S. Karuppanan, H.J. Kim, K. Prabakar, Open atmospheric processed perovskite solar cells using dopant-free, highly hydrophobic hole-transporting materials: influence of thiophene and selenophene π-spacers on charge transport and recombination properties, Sol. Energy Mater. Sol. Cells 199 (2019) 66–74, https://doi.org/10.1016/j.solmat.2019.04.026.

[30] P. Guo, J. Sun, S. Sun, J. Li, J. Tong, C. Zhao, L. Zhu, P. Zhang, C. Yang, Y. Xia, Effect of alkylthiophene spacers and fluorine on the optoelectronic properties of 5,10-bis(dialkylthien-2-yl)dithieno[2,3-d:2′,3′- d ′]benzo[1,2-b:4,5- b ′] dithiophene- alt -benzothiadiazole derivative copolymers, RSC Adv. 7 (2017) 22845–22854, https://doi.org/10.1039/c6ra28836g.

[31] Z. Liang, M. Li, X. Zhang, Q. Wang, Y. Jiang, H. Tian, Y. Geng, Near-infrared absorbing non-fullerene acceptors with selenophene as π bridges for efficient organic solar cells, J. Mater. Chem. A. 6 (2018) 8059–8067, https://doi.org/10.1039/c8ta00783g.

[32] D. Keles, M.C. Erer, E. Bolayir, S.C. Cevher, G. Hizalan, L. Toppare, A. Cirpan, Conjugated polymers with benzothiadiazole and benzotriazole moieties for polymer solar cells, Renew. Energy 139 (2019) 1184–1193, https://doi.org/10.1016/j.renene.2019.03.018.

[33] W. Wu, J. Li, F. Guo, L. Zhang, Y. Long, J. Hua, Photovoltaic performance and long-term stability of quasi-solid-state fluoranthene dyes-sensitized solar cells, Renew. Energy 35 (2010) 1724–1728, https://doi.org/10.1016/j.renene.2009.11.021.

[34] X. Zhang, Q. Wang, Z. Liang, M. Li, Y. Geng, Low-bandgap non-fullerene acceptors based on selenophene π spacer and alkylated indaceno[1,2-b:5,6-b′] dithiophene for organic solar cells, Org, Electron 69 (2019) 200–207, https://doi.org/10.1016/j.orgel.2019.03.038.

[35] S. Pang, R. Zhang, C. Duan, S. Zhang, X. Gu, X. Liu, F. Huang, Y. Cao, Alkyl chain length effects of polymer donors on the morphology and device performance of polymer solar cells with different acceptors, Adv. Energy Mater. 9 (2019) 1–12, https://doi.org/10.1002/aenm.201901740.

[36] Y. Yu, N. Wang, B. Meng, J. Liu, L. Wang, Effect of alkyl side chains of polymer donors on photovoltaic performance of all-polymer solar cells, ACS Appl. Polym. Mater. 3 (2021) 42–48, https://doi.org/10.1021/acsapm.0c00766.

[37] S. Kouijzer, J.J. Michels, M. Van Den Berg, V.S. Gevaerts, M. Turbiez, M.M. Wienk, R.A.J. Janssen, Predicting morphologies of solution processed polymer:Fullerene blends, J. Am. Chem. Soc. 135 (2013) 12057–12067, https://doi.org/10.1021/ja405493j.

[38] J.J. Van Franeker, M. Turbiez, W. Li, M.M. Wienk, R.A.J. Janssen, A real-time study of the benefits of co-solvents in polymer solar cell processing, Nat. Commun. 6 (2015) 1–8, https://doi.org/10.1038/ncomms7229.

[39] C. Wang, K. Nakano, H.F. Lee, Y. Chen, Y.L. Hong, Y. Nishiyama, K. Tajima,

Intermolecular arrangement of fullerene acceptors proximal to semiconducting polymers in mixed bulk heterojunctions, Angew. Chem. Int. Ed. 57 (2018) 7034–7039, https://doi.org/10.1002/anie.201801173.
[40] X. Bi, T. Zhang, C. An, P. Bi, K. Ma, S. Li, K. Xian, Q. Lv, S. Zhang, H. Yao, B. Xu, J. Zhang, S. Cao, J. Hou, Enhanced photovoltaic effect from naphtho[2,3-: C] thiophene-4,9-dione-based polymers through alkyl side chain induced backbone distortion, J. Mater. Chem. A. 8 (2020) 14706–14712, https://doi.org/10.1039/d0ta02859b.
[41] J. Zhao, Q. Li, S. Liu, Z. Cao, X. Jiao, Y.P. Cai, F. Huang, Bithieno[3,4- c]pyrrole-4,6-dione-Mediated crystallinity in large-bandgap polymer donors directs charge transportation and recombination in efficient nonfullerene polymer solar cells, ACS Energy Lett (2020) 367–375, https://doi.org/10.1021/acsenergylett.9b02842.
[42] W.T. Hadmojo, F.T.A. Wibowo, D.Y. Ryu, I.H. Jung, S.Y. Jang, Fullerene-free organic solar cells with an efficiency of 10.2% and an energy loss of 0.59 eV based on a thieno[3,4-c]Pyrrole-4,6-dione-containing wide band gap polymer donor, ACS Appl. Mater. Interfaces 9 (2017) 32939–32945, https://doi.org/10.1021/acsami.7b09757.
[43] J. Ha, C.E. Song, H.S. Kim, D.H. Ryu, W.S. Shin, D. Hwang, Highly E ffi cient and photostable ternary organic solar cells enabled by the combination of non-fullerene and fullerene acceptors with thienopyrrolodione-based polymer donors, ACS Appl. Mater. Interfaces (2020), https://doi.org/10.1021/acsami.0c14367.
[44] F. Yang, W. Zhao, Q. Zhu, C. Li, W. Ma, J. Hou, W. Li, Boosting the performance of non-fullerene organic solar cells via cross-linked donor polymers design, Macromolecules 52 (2019) 2214–2221, https://doi.org/10.1021/acs.macromol.8b02526.
[45] C.H. Zhang, W. Wang, W. Huang, J. Wang, Z. Hu, Z. Lin, T. Yang, F. Lin, Y. Xing, J. Bai, H. Sun, Y. Liang, Methyl thioether functionalization of a polymeric donor for efficient solar cells processed from non-halogenated solvents, Chem. Mater. 31 (2019) 3025–3033, https://doi.org/10.1021/acs.chemmater.9b00926.
[46] F. Lin, W. Huang, H. Sun, J. Xin, H. Zeng, T. Yang, M. Li, X. Zhang, W. Ma, Y. Liang, Thieno[3,4-c]pyrrole-4,6(5H)-dione polymers with optimized energy level alignments for fused-ring electron acceptor based polymer solar cells, Chem. Mater. 29 (2017) 5636–5645, https://doi.org/10.1021/acs.chemmater.7b01335.
[47] H. Hwang, C. Park, D.H. Sin, E. Song, K. Cho, High absorption coefficient π-conjugation-extended donor-acceptor copolymers for ternary-blend solar cells, Org. Electron. 83 (2020) 105738, https://doi.org/10.1016/j.orgel.2020.105738.
[48] B. Zhao, H. Wu, W. Wang, H. Liu, J. Liu, Z. Cong, C. Gao, Efficient non-fullerene polymer solar cells enabled by side-chain conjugated thieno[3,4-c]pyrrole-4,6-dione-based polymer and small molecular acceptors, React. Funct. Polym. 145 (2019) 104378, https://doi.org/10.1016/j.reactfunctpolym.2019.104378.
[49] J.S. Park, G.U. Kim, D. Lee, S. Lee, B. Ma, S. Cho, B.J. Kim, Importance of optimal crystallinity and hole mobility of BDT-based polymer donor for simultaneous enhancements of Voc, jsc, and FF in efficient nonfullerene organic solar cells, Adv. Funct. Mater. 2005787 (2020) 1–9, https://doi.org/10.1002/adfm.202005787.
[50] M. Yasa, A. Deniz, M. Forough, E. Yildirim, O. Persil Cetinkol, Y.A. Udum, L. Toppare, Construction of amperometric biosensor modified with conducting polymer/carbon dots for the analysis of catechol, J. Polym. Sci. (2020) 1–13, https://doi.org/10.1002/pol.20200647.
[51] E. Zhou, J. Cong, K. Tajima, C. Yang, K. Hashimoto, Conjugated polymers based on 1,3-dithien-2-yl-thieno[3,4- c]pyrrole-4,6-dione: synthesis, characterization, and solvent effects on photovoltaic performance, J. Phys. Chem. C 116 (2012) 2608–2614, https://doi.org/10.1021/jp209253m.
[52] J. Huang, Y. Zhao, W. He, H. Jia, Z. Lu, B. Jiang, C. Zhan, Q. Pei, Y. Liu, J. Yao, Effects of structure-manipulated molecular stacking on solid-state optical properties and device performances, Polym. Chem. 3 (2012) 2832–2841, https://doi.org/10.1039/c2py20406a.
[53] Y.S. Park, E. Kim, B. Hong, J. Lee, Characteristics of ITO films with oxygen plasma treatment for thin film solar cell applications, Mater. Res. Bull. 48 (2013) 5115–5120, https://doi.org/10.1016/j.materresbull.2013.07.026.
[54] Z. Zhang, T. Wang, Z. Ding, J. Miao, J. Wang, C. Dou, B. Meng, J. Liu, L. Wang, Small molecular donor/polymer acceptor type organic solar cells: effect of molecular weight on active layer morphology, Macromolecules 52 (2019) 8682–8689, https://doi.org/10.1021/acs.macromol.9b01666.
[55] Z. Li, W. Zhong, L. Ying, F. Liu, N. Li, F. Huang, Y. Cao, Morphology optimization via molecular weight tuning of donor polymer enables all-polymer solar cells with simultaneously improved performance and stability, Nanomater. Energy 64 (2019) 103931, https://doi.org/10.1016/j.nanoen.2019.103931.
[56] V.D. Mihailetchi, P.W.M. Blom, J.C. Hummelen, M.T. Rispens, Cathode dependence of the open-circuit voltage of polymer:fullerene bulk heterojunction solar cells, J. Appl. Phys. 94 (2003) 6849–6854, https://doi.org/10.1063/1.1620683.
[57] X. Guo, M. Zhang, L. Huo, F. Xu, Y. Wu, J. Hou, Design, synthesis and photovoltaic properties of a new D-π-A polymer with extended π-bridge units, J. Mater. Chem. 22 (2012) 21024–21031, https://doi.org/10.1039/c2jm32931j.
[58] G. Bernardo, G. D, Recent progress in the understanding and manipulation of morphology in polymer: fullerene photovoltaic cells, optoelectron, Adv. Mater. Devices (2013), https://doi.org/10.5772/51115.
[59] Y. Lu, Y. Wang, Z. Feng, Y. Ning, X. Liu, Y. Lü, Y. Hou, Temperature-dependent morphology evolution of P3HT:PCBM blend solar cells during annealing processes, Synth. Met. 162 (2012) 2039–2046, https://doi.org/10.1016/j.synthmet.2012.10.012.
[60] X. Song, N. Gasparini, D. Baran, The influence of solvent additive on polymer solar cells employing fullerene and non-fullerene acceptors, Adv. Electron. Mater. 4 (2018) 1–7, https://doi.org/10.1002/aelm.201700358.
[61] S. Beaupré, S. Shaker-Sepasgozar, A. Najari, M. Leclerc, Random D-A1-D-A2 terpolymers based on benzodithiophene, thiadiazole[3,4-e]isoindole-5,7-dione and thieno[3,4-c]pyrrole-4,6-dione for efficient polymer solar cells, J. Mater. Chem. A. 5 (2017) 6638–6647, https://doi.org/10.1039/c7ta01467h.
[62] V. Tamilavan, K.H. Roh, R. Agneeswari, D.Y. Lee, S. Cho, Y. Jin, S.H. Park, M.H. Hyun, Highly efficient imide functionalized pyrrolo[3,4-c]-pyrrole-1,3-dione-based random copolymer containing thieno[3,4-c]pyrrole-4,6-dione and benzodithiophene for simple structured polymer solar cells, J. Mater. Chem. A. 2 (2014), https://doi.org/10.1039/c4ta05086j, 20126–20132.
[63] E. Zhou, J. Cong, K. Hashimoto, K. Tajima, Introduction of a conjugated side chain as an effective approach to improving donor-acceptor photovoltaic polymers, Energy Environ. Sci. 5 (2012) 9756–9759, https://doi.org/10.1039/c2ee23383e.
[64] Ö. Azeri, E. Aktas, C. Istanbulluoglu, S.O. Hacioglu, S.C. Cevher, L. Toppare, A. Cirpan, Efficient benzodithiophene and thienopyrroledione containing random polymers as components for organic solar cells, Polymer 133 (2017) 60–67, https://doi.org/10.1016/j.polymer.2017.11.024.
[65] G. Zhang, Y. Fu, L. Qiu, Z. Xie, Synthesis and characterization of thieno[3,4-c] pyrrole-4,6-dione and pyrrolo[3,4-c]pyrrole-1,4-dione-based random polymers for photovoltaic applications, Polymer 53 (2012) 4407–4412, https://doi.org/10.1016/j.polymer.2012.08.011.
[66] A.A. Advincula, I. Pelse, J.R. Reynolds, Side chain independent photovoltaic performance of thienopyrroledione conjugated donor-acceptor polymers, J. Mater. Chem. C. 8 (2020) 16452–16462, https://doi.org/10.1039/d0tc03883k.